This manuscript was accepted by Rev. Sci.Instrum. Click here to see the version of record.

A new toroidal x-ray crystal spectrometer for the diagnosis of high energy density plasmas at the National Ignition Facility[a)]

M. Bitter,[1,b)] K. W. Hill,[1] LanGao,[1] B. F. Kraus,[1] P. C. Eftihimion,[1] L. Delgado-Apericio,[1] N. Pablant,[1] B. Stratton,[1] M. Schneider,[2] F. Coppari,[2] R. Kauffman,[2] A. G. MacPhee,[2] Y. Ping,[2] and D. Thorn[2]

[1]*Princeton Plasma Physics Laboratory, Princeton, New Jersey 08543, USA*
[2]*Lawrence Livermore National Laboratory, Livermore, California 94550, USA*

(Presented XXXXX; received XXXXX; accepted XXXXX; published online XXXXX)
(Dates appearing here are provided by the Editorial Office)

The here-described spectrometer was developed for the Extended X-ray Absorption Fine Structure (EXAFS) spectroscopy of high-density plasmas at the National Ignition Facility (NIF). It employs as the Bragg reflecting element at new type of toroidally bent crystal with a constant and very large major radius R and a much smaller, locally varying, minor radius r. The focusing properties of this crystal and the experimental arrangement of source and detector make it possible to **(a)** fulfill the conditions for a perfect imaging of an ideal point source for each wavelength, **(b)** obtain a high photon throughput, **(c)** obtain a high spectral resolution by eliminating the effects of source-size broadening, and **(d)** obtain a one-dimensional spatial resolution with a high magnification perpendicular to the main dispersion plane.

I. INTRODUCTION

X-ray diffraction (XRD) and the Extended X-ray Absorption Fine Structure (EXAFS) spectroscopy are among the most widely used diagnostics in high pressure condensed matter studies because of their capability to provide information about the structural transformations occurring in the material at the atomic level. Developing these techniques to study samples that have been ramp-compressed to very high pressures will extend knowledge of matter at extreme conditions. These conditions can be achieved using large lasers to do the compression, such as the NIF lasers at Lawrence Livermore National Laboratory or the OMEGA laser at the Laboratory for Laser Energetics (Rochester, NY).[1] A major challenge for the EXAFS spectroscopy at these facilities is, however, the development of a spectrometer, which satisfies the simultaneous requirements of a high spectral resolution and a high photon-throughput, for an extended spectral range. Notably, the effects of source-size broadening, which limit the spectral resolution, have been so troubling that, ultimately, in order to mitigate these effects, painstaking 'source development' experiments were conducted at the NIF to reduce the source size itself.[1,2]

An important step towards a solution of the source-size broadening problem by an improved spectrometer design was made by J. Koch,[3] who proposed the use of a modified Johann spectrometer with a spherical Ge-220 crystal of a large radius of **R** = 4826 mm, where the x-ray source would be close to the crystal to enhance the photon-throughput and where the detector would be placed on the Rowland circle – see Fig. 1 - to eliminate the effects of source-size broadening, since - at the Rowland circle - the separation of the rays, which emanate from different points of an extended source and which are Bragg reflected with the same Bragg angle **Θ**, is minimal.

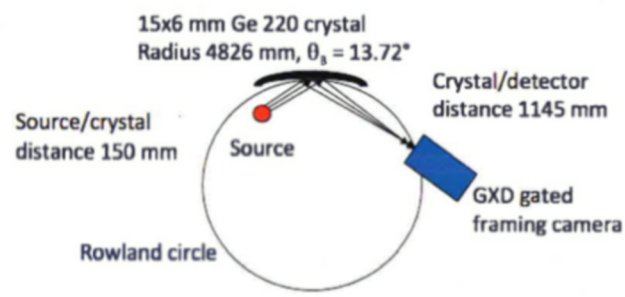

FIG. 1. Original Figure from Koch's proposal[3]. – We point out that the parameter values used in FIG. 1 differ from those which are quoted. The Bragg angle, source-crystal distance, and crystal-detector distance, shown, are 35° (instead of 13.72°), 1380 mm (instead of 150 mm), and 2768 mm (instead of 1145 mm), respectively.

Koch's spectrometer design had, however, two shortcomings:

1. The distance, $d_{SC} = 150mm$, of the source from the central point on the crystal surface was much shorter than the crystal's sagittal focal length, which - for the main Bragg angle in Koch's design of $\theta_0 = 13.72°$– amounted to $f_s = \frac{R}{2 \bullet \sin(\theta_0)} = 10174mm$. The image of the source was

[a)]Published as part of the Proceedings of the 22nd Topical Conference on High-Temperature Plasma Diagnostics (HTPD 2018) in San Diego, California, USA.
[b)]Author to whom correspondence should be addressed: bitter@pppl.gov

This manuscript was accepted by Rev. Sci.Instrum. Click here to see the version of record.

therefore a virtual image, which was located behind the crystal, at the distance, $d_{IM} = 152.24mm$, from the central point on the crystal's surface. The reflected rays, which seem to emanate from this virtual image, were therefore divergent and their points of intersection with the detector plane were spread out on an elliptical arc of the length **H**, which was determined by the height **h** of the crystal:

$$H = \frac{d_{IM} + R \bullet \sin(\theta_0)}{d_{IM}} \bullet h = 8.5 \bullet h$$

so that for a modest height of the crystal of $h = 10mm$, the height of the detector needed to be $H = 85mm$ in order to collect all the reflected photons. The useful height of the crystal and hence the attainable photon throughput were thus ultimately limited by the height **H** of the detector. – It is not possible to increase the photon throughput beyond this limit by moving the source still closer to the crystal, since the reflected rays are then even more divergent. - The realization of Koch's idea of increasing the photon throughput by moving the source close to the crystal is, therefore, actually very much constrained.

2. Koch's other suggestion, namely, to eliminate the source-size broadening effects by placing the detector on the Rowland circle, is not specific enough and for his chosen orientation of the detector plane - perpendicular to the main reflected ray for the Bragg angle $\theta_0 = 13.72°$- the source-size broadening effects are only eliminated for the wavelength, which is associated with the Bragg angle θ_0, but not for the entire spectral range.

Our new spectrometer design, which is described in section II, eliminates these shortcomings of Koch's design and satisfies the imaging conditions for each wavelength perfectly. Also, the effects of source-size and crystal-thickness broadening are eliminated for the entire spectral range of interest by positioning the detector at the tangency point of the proper tangency circle (see section II) for each wavelength. Thus, it is possible to obtain at once a high photon throughput, a high spectral resolution, and a one-dimensional spatial resolution perpendicular to the main dispersion plane with a high magnification.

II. A NEW EXAFS SPECTROMETER

A. Spectrometer Design

FIG. 2 shows the ray pattern for Koch's design in more detail and introduces the concept of the 'tangency circle', which is used for our new design. The point **O** is the center of the crystal sphere and a center of symmetry, since any straight line through **O** is an axis of rotational symmetry that can be used for imaging. Since the imaging conditions require that the point source **S** and its image point **I** are fixed points with respect to a rotation of the ray pattern, these points must be on an axis of rotation, which - in the case of a sphere - must also pass through **O**. This axis of rotational symmetry is therefore uniquely defined if the position of the source **S** is given. The image **I** is then at the point of intersection of the axis of rotation with the reflected ray. For Koch's design, the image **I** is a virtual image, which is located behind the crystal, see FIG. 2. By rotating the ray pattern in FIG. 2 about the axis **OSI**, one can easily visualize that the reflected rays describe a cone with the apex at **I**. The reflected rays are, therefore, divergent and their points of intersection with a detector plane, which is oriented along **OU** and perpendicular to the main dispersion plane describe a conic section, which is often an ellipse.

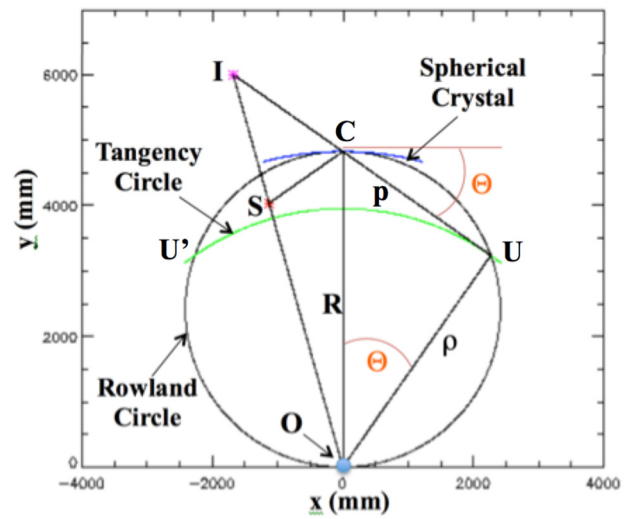

FIG. 2. More detailed ray pattern for Koch's design, using the actual dimensions of FIG. 1.

We also infer from FIG. 2 that the reflected ray in the main dispersion plane is - at its intersection point **U** with the Rowland circle - tangential to the circle with the radius $\rho = R\cos(\theta)$ about **O**, since the distance of **CU** is equal to $p = R\sin(\theta)$ and since the Rowland circle is Thales' circle. The points **U'** and **U**, which are usually described as the intersection points of the incident and reflected rays with the Rowland circle, can therefore also be defined as the tangency points of the incident and reflected rays on the sphere with the radius $\rho = R\cos(\theta)$ about **O**; the green circle in FIG. 2 is then the trace of this sphere in the main dispersion plane. The definitions of the Rowland circle and the tangency sphere are substantially different: The tangency sphere maintains the spherical symmetry of the ray pattern, since it is concentric with the crystal sphere. It can therefore conveniently be used to describe the incident and reflected rays at each crystal point, for a given Bragg angle **Θ**. By contrast, the definition of the Rowland circle breaks the spherical symmetry by singling out a particular crystal point, e.g., the point **C** in FIG. 2, since the Rowland circle passes through **O** and a particular point of Bragg reflection. In principle, one must define a Rowland circle for each crystal point, so that there is an infinite number of equivalent Rowland circles.

This manuscript was accepted by Rev. Sci.Instrum. Click here to see the version of record.

The concept of the 'tangency' sphere is also useful for a description of the ray pattern from an extended source, a derivation of the Johann error and an understanding of the source-size broadening effects. For this purpose, we consider in FIG. 3, the ray pattern from an extended source for the Bragg angle **Θ** = 59° > 45°, where the images **I** are real. The ray pattern, shown in FIG. 3, is actually a superposition of the identical ray patterns from three source points $\mathbf{S_0}$, $\mathbf{S_1}$, and $\mathbf{S_2}$ of an extended source. The points $\mathbf{C_0}$, $\mathbf{C_1}$, $\mathbf{C_2}$ and $\mathbf{U_0}$, $\mathbf{U_1}$, $\mathbf{U_2}$ are, respectively, the points of Bragg reflection and the tangency points for the reflected rays on the tangency circle with $\rho = R\cos(\theta)$. The points $\mathbf{U_0}$, $\mathbf{U_1}$, $\mathbf{U_2}$ are also the positions of the real images $\mathbf{I_0}$, $\mathbf{I_1}$, $\mathbf{I_2}$. Since the three ray patterns are identical, they can be made congruent by a rotation about an axis through **O** that is perpendicular to the drawing plane of FIG. 3 by an angle **α**. We infer from FIG. 3 that the reflected rays from $\mathbf{C_1}$ (red ray) and $\mathbf{C_2}$ (green ray) intersect each other at a point outside of and at a distance **ξ** from the tangency circle, on the extension of the line segment $\mathbf{OU_0}$. This distance ξ is given by the equation, $(\rho+\xi)\cos(\alpha)=\rho$; and the solution of this equation, if **ξ** and **α** can be considered as small quantities, is the well-known Johann error: $\xi = \rho\frac{\alpha^2}{2} = \frac{w^2}{8R}\cos(\theta)$, where **α** has been expressed by the width $\mathbf{w} = \mathbf{C_1C_2}$ of the crystal.

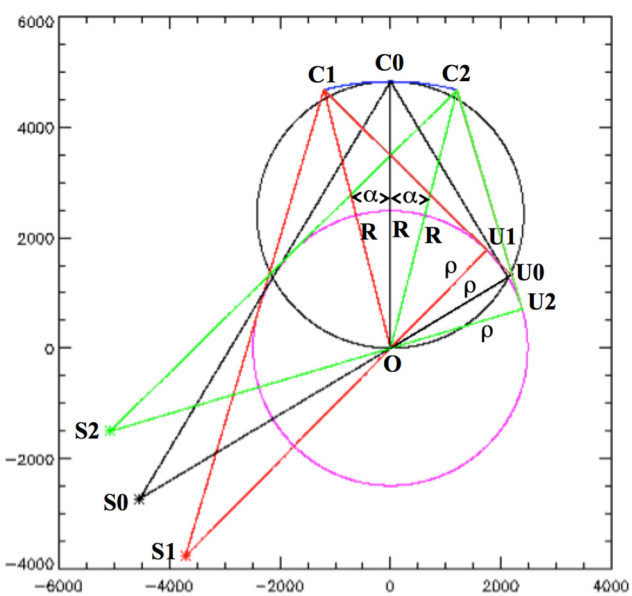

FIG. 3. Ray pattern for the Bragg angle Θ = 59° and three source points $\mathbf{S_0}$, $\mathbf{S_1}$, and $\mathbf{S_2}$ of an extended source.

The Johann error is the minimum separation between the rays, which emanate from an extended source and which are Bragg reflected from a spherical crystal of the width **w** with the Bragg angle **Θ**. This minimum occurs at the tangency point $\mathbf{U_0}$, which is therefore the preferred detector position, if it is necessary to eliminate source-size broadening effects in order to enhance the spectral resolution. Evidently, the spatial extension of a source will not be noticeable if the detector is placed at $\mathbf{U_0}$ and if the Johann error is smaller than the detector resolution.

Also the detrimental effects to the spectral resolution which result from the penetration of the x-rays to lattice planes deep inside the crystal, the so-called crystal-thickness broadening, can be minimized by positioning the detector at $\mathbf{U_0}$, since the Bragg reflection from those lattice planes leads to a lateral displacement of the exiting (Bragg reflected) ray from the incident ray on the front surface of the crystal that is similar to the displacement between the Bragg reflection points ($\mathbf{C_1}$ and $\mathbf{C_2}$ in FIG 3) in the case of an extended source. The crystal-thickness broadening leads thus to an additional Johann error at $\mathbf{U_0}$ that could be subsumed in the Johann error, which results from the spatial extension of the source.

In the following, we describe our design of an EXAFS spectrometer for the x-ray energies $8.877 \le E \le 10.877 keV$ which include the energy of the TaL_3 absorption edge at 9.877 keV. Our design is based on Koch's original design. But, instead of a spherical crystal, we use a toroidally bent crystal with a varying minor radius. This special crystal shape evolved from an application of basic physics principles as we tried to satisfy the imaging conditions for each wavelength and to generate a real image, at the tangency point of the reflected rays with the proper tangency spheres. The essential features of our design are shown in FIG. 4 and are further explained below.

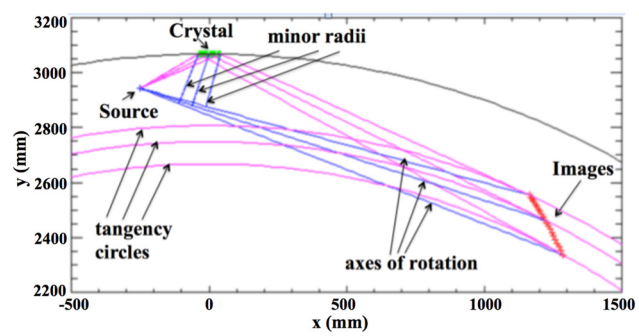

FIG. 4. Arrangement of source, crystal and image points in the main dispersion plane (x,y-plane).

The crystal is a Ge[400]-crystal with the 2d-lattice spacing of $2d = 2.82868 Å$ and a large major radius **R** = 3068 mm. Its trace in the main dispersion plane is shown by the black circle with the radius **R** about the point (x=0; y=0). Also, similar to Koch's design, the source is placed at a short distance, $d_{SC} = 280 mm$, from the central point (x=0; y=R) on the crystal surface. The points, shown in green, represent 21 crystal points, which are the points of Bragg reflection for 21 equidistant x-ray energies in the interval from 8.877 to 10.877 keV. The central crystal point at x=0, y=**R** is associated with the energy E=9.877 keV of the TaL_3 absorption edge. The points, shown in red, are the tangency points of the Bragg reflected rays in the main dispersion plane with the circles of the radii

This manuscript was accepted by Rev. Sci.Instrum. Click here to see the version of record.

$\rho = R \bullet \cos(\theta)$ about x=0,y=0 for those 21 x-ray energies. Only three of these tangency circles, for the energies E = 8.877; 9.877; 10.877 keV and the corresponding Bragg angles Θ = 29.588; 26.345; 24.482°, are shown in magenta in FIG. 4 together with the incident and reflected rays. In order to create, for each wavelength, a real image of the source at the tangency point for the Bragg reflected ray with the proper tangency circle in the main dispersion plane, we demand that the interconnecting straight (blue) lines between the source and the tangency point for each wavelength are axes of rotational symmetry for the crystal. The source point and the tangency points are then fixed points with respect to rotations of the ray patterns for each wavelength about those axes. The short line segments *(blue)*, which are normal to these axes of rotational symmetry and which extend from these axes up to the points of Bragg reflection, represent the locally varying minor radii **r** of a toroidally bent crystal. We point out that according to the above given formula, the Johann error at the here defined image points, would only be about 0.3 µm, for a relatively large, 2 mm wide, extended source and our design parameters.

B. Dispersion

The wavelength dispersion is defined as $\frac{d\lambda}{ds}$, where λ is the wavelength and where s is the length of arc on which the image points are distributed in the main dispersion plane. We use the following formulas:

$$(1) \qquad ds = \sqrt{1+\left(\frac{dy_I}{dx_I}\right)^2} \bullet dx_I$$

where x_I and y_I are the coordinates of the image points in the main dispersion plane. Equation (1) can be rewritten as

$$(2) \qquad \frac{ds}{d\lambda} = \sqrt{1+\left(\frac{dy_I}{dx_I}\right)^2} \bullet \frac{dx_I}{d\lambda}$$

FIGS. 5 and 6 show the functions $y_i(x_I)$ and $x_i(\lambda)$ on enlarged scales and demonstrate that, for the parameters of our present design, these functions are well approximated by straight lines with the slopes $\frac{dy_I}{dx_I} = -1.79$ and $\frac{dx_I}{d\lambda} = 474.77[mm/\AA]$. Inserting these numerical values in eq. (2), we get

$$(2') \qquad \frac{ds}{d\lambda} = 972.12[mm/\AA]$$

and

$$(1') \qquad \frac{d\lambda}{ds} = 1.03\ [m\AA/mm]$$

The resolving power derived from eq. (1') for the case that the detector is an image plate, assuming a 100 µm detector resolution, is 12000, which should be sufficient to accurately measure the EXAFS oscillations near the TaL3 absorption edge, since the period of theses oscillations is about 50 eV – see FIG. 5c in ref [6] and FIG. 9b in ref. [7].

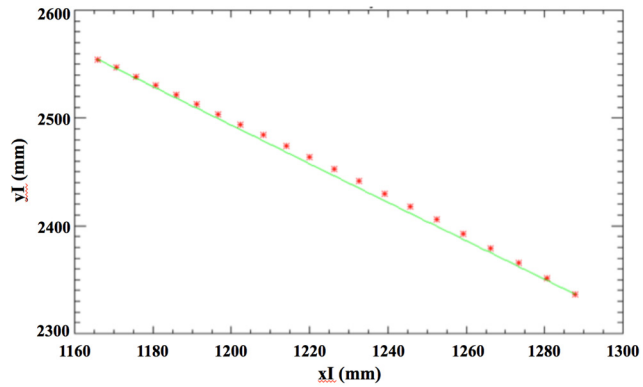

FIG. 5. Image points in the detector plane *(red)* and the straight line *(green)* connecting the end points (x_I=1165.93 mm, y_I=2554.36 mm) and (x_I=1287.86 mm, y_I=2336.51 mm).

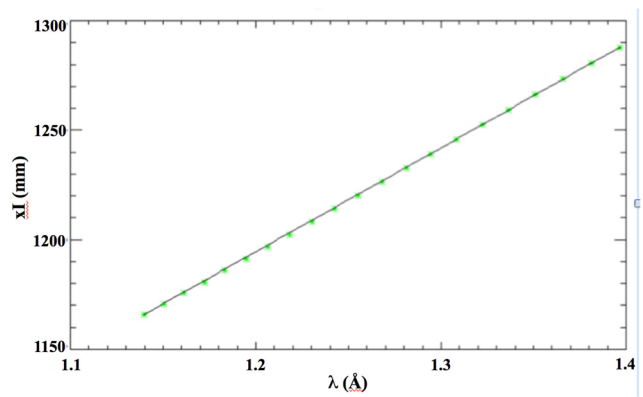

FIG. 6. Abscissa x_I of image points *(green)* as a function of λ and straight line *(blue)* connecting the endpoints.

The required length of the detector to cover the energy range, 8.877 < E < 10.877 keV, is:

$$(3) \qquad s = \frac{ds}{d\lambda} \bullet (\lambda_1 - \lambda_2) = 249.7mm$$

where $\lambda_1 = 1.39669\AA$ and $\lambda_2 = 1.13987\AA$ correspond to the x-ray energies of 8.877 and 10,877 keV.

C. Spatial Resolution

Our spectrometer design also provides a 1D spatial resolution with a magnification **M**, given by

$$(4) \quad M = \frac{R\sin(\theta)\cos(\theta)}{d_{SC}\cos(\theta)} = \frac{R}{d_{SC}}\sin(\theta)$$

This manuscript was accepted by Rev. Sci.Instrum. Click here to see the version of record.

III. DISCUSSION AND CONCLUSIONS

The novelty of our spectrometer a toroidally bent crystal with a varying minor radius, which changes in magnitude and direction along the crystal surface to establish, at each crystal point, the proper rotational symmetry for the imaging of an ideal point source. The axis of the rotational symmetry and the minor radius are at each crystal point uniquely defined by the law of Bragg reflection and the positions of source and image on the incident and reflected rays. In particular, one can choose a source position close to the crystal to enhance the photon throughput and then generate, for each wavelength, a real image at the point with the minimum Johann aberration in order to eliminate the effects of source-size broadening. In doing so, one obtains not only a high spectral resolution but also a high spatial resolution perpendicular to the main dispersion plane. - We point out that, in Koch's design, the divergence of the reflected rays precludes the possibility of obtaining a spatial resolution. – Our new toroidal crystal spectrometer offers, therefore, a high degree of flexibility and new features that are unmatched by any of the existing spectrometers. In fact, the toroidal crystal spectrometers, which are presently being used for the diagnosis of laser-produced plasmas – see, e.g. E. J. Gamoa et al. [4] - are distinctly different from our spectrometer due to the fact that these spectrometers use a conventional toroidal crystal form with a constant minor radius which at every crystal point is aligned with the normal to the crystal surface.

The differences between our spectrometer and the traditional toroidal crystal spectrometer are further explained with aid of FIG. 4, where the *black* circles with the radii **R** = 400 mm about **O** and $\mathbf{R_R = R/2}$ about **M** represent the trace of a toroidal crystal and the Rowland circle in the main dispersion plane. The crystal point **C** is the point of Bragg reflection. The ray, which is incident on **C** with the Bragg angle **Θ**, is assumed to emanate from an ideal point source that may be positioned at $\mathbf{S_1}$ or $\mathbf{S_2}$. We demand that the image of $\mathbf{S_1}$ or $\mathbf{S_2}$ is a real image at the point **I** on the Rowland circle.

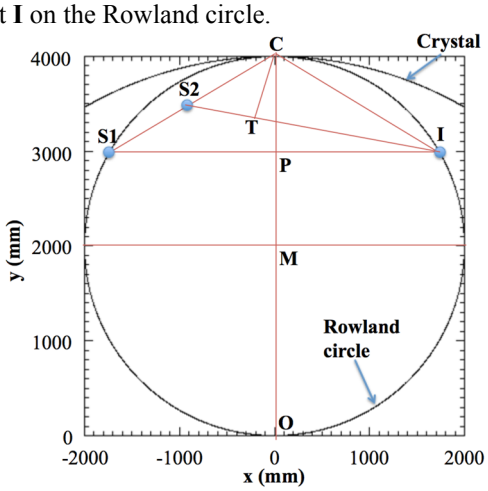

FIG. 7. Illustration of the differences between a torus with varying minor radius and a conventional torus.

In the case of a conventional torus, the major and minor radii, $\mathbf{R_t}$ and $\mathbf{r_t}$, are perfectly aligned with each other in the main dispersion plane. The axis, associated with the rotational symmetry of the ray pattern, must therefore be perpendicular to the straight line from **O** to **C** and pass through **I** and $\mathbf{S_1}$, since the source and image points must be on the axis of rotation. It then follows that **I** and $\mathbf{S_1}$ have to be both on the Rowland circle; and the major and minor radii must be equal to $\mathbf{R_t = OP}$ and $r_t = CP = R \bullet \sin^2(\theta)$, since the distances of $\mathbf{S_1}$ and **I**, from the point of Bragg reflection **C**, are equal to $R \bullet \sin(\theta)$. With a conventional toroidal crystal, one can simultaneously satisfy the conditions for imaging and eliminate the effects of source-size broadening for only one particular wavelength λ. The associated Bragg angle, Θ(λ), and minor radius, $\mathbf{r_t(\lambda)}$, must fulfill the relation $r_t = R\sin^2\left(\theta(\lambda)\right)$. For this particular wavelength λ, one also obtains, a 1D spatial resolution perpendicular to the main dispersion plane with the magnification of **M** = 1. However, for any other wavelength and any other source and detector position, the basic physics principles for imaging are violated.

On the other hand, it is possible to construct, for any given image point **I** and source point $\mathbf{S_2}$ a torus with varying minor radius $r_t = CT$ - *see FIG. 7*- such that the Bragg condition and the imaging conditions are fulfilled; and, as we have shown in this paper, this can be done for each wavelength in an extended spectral range.

Our spectrometer design for EXAFS studies of the TaL_3 absorption edge will be tested at the Laboratory for Laser Energetics (LLE) in Rochester during this fall and then, depending on the outcome of this test, also be used at the NIF. The specifications and procedures for the manufacture and alignment of a toroidal crystal with varying minor radius are presently being defined and will be described in a subsequent paper.

IV. ACKNOWLEDGEMENTS

This work was performed under the auspices of the U. S. DoE by LLNL under Contract DE-AC52-07NA27344 and PPPL under contract DE-AC02-09CH11466.

[1]F. Coppari, D. B. Thorn, G. E. Kemp, R. S. Craxton, E. M. Garcia, Y. Ping, J. H. Eggert, and M. B. Schneider, Rev. Sci. Instrum. **88**, 083907 (2017).
[2]A. Krygier et al., poster at this conference: "Developing a bright, high-energy continuum backlighter for EXAFS on NIF"
[3]J. Koch, LLNL X-ray Spectroscopy Workshop 2015.
[4]E. J. Gamboa, C. M. Huntington, M. R. Trantham, P. A. Keiter, R. P. Drake, D. S. Montgomery, J. F. Benage, and S. A. Letzring, Rev. Sci. Instrum. **83**, 10E108 (2012).
[5] Y. Ping, D. G. Hicks, B. Yaakobi, F. Coppari, J. Eggert, and G. W. Collins, Rev. Sci. Instrum. **84**, 123105 (2013).
[6] Yuan Ping and Federica Coppari, HIGH PRESSURE RESEARCH, DOI: 10180/08957959.2016.1196203
http://dx.doi.org/10.1080/08957959.2016.1196203

This manuscript was accepted by Rev. Sci.Instrum. Click here to see the version of record.